

ClearAIR: A Human-Visual-Perception-Inspired All-in-One Image Restoration

Xu Zhang¹, Huan Zhang², Guoli Wang³, Qian Zhang³, Lefei Zhang^{1*}

¹National Engineering Research Center for Multimedia Software, School of Computer Science, Wuhan University

²School of Information Engineering, Guangdong University of Technology

³Horizon Robotics

{zhangx0802, zhanglefei}@whu.edu.cn, huanzhang2021@gdut.edu.cn, {guoli.wang, qian01.zhang}@horizon.auto

Abstract

All-in-One Image Restoration (AiOIR) has advanced significantly, offering promising solutions for complex real-world degradations. However, most existing approaches rely heavily on degradation-specific representations, often resulting in oversmoothing and artifacts. To address this, we propose ClearAIR, a novel AiOIR framework inspired by Human Visual Perception (HVP) and designed with a hierarchical, coarse-to-fine restoration strategy. First, leveraging the global priority of early HVP, we employ a Multi-modal Large Language Model (MLLM)-based Image Quality Assessment (IQA) model for overall evaluation. Unlike conventional IQA, our method integrates cross-modal understanding to more accurately characterize complex, composite degradations. Building upon this overall assessment, we then introduce a region awareness and task recognition pipeline. A semantic cross-attention, leveraging semantic guidance unit, first produces coarse semantic prompts. Guided by this regional context, a degradation-aware module implicitly captures region-specific degradation characteristics, enabling more precise local restoration. Finally, to recover fine details, we propose an internal clue reuse mechanism. It operates in a self-supervised manner to mine and leverage the intrinsic information of the image itself, substantially enhancing detail restoration. Experimental results show that ClearAIR achieves superior performance across diverse synthetic and real-world datasets.

Introduction

Image restoration aims to recover a clean image from its degraded version and has made significant progress with deep learning. Early approaches employed task-specific networks for individual degradation types, such as denoising (Martin et al. 2001), dehazing (Shi et al. 2025; Li et al. 2018), deraining (Jiang et al. 2020), deblurring (Nah, Hyun Kim, and Mu Lee 2017; Li et al. 2024a), and low-light enhancement (Wei et al. 2018), achieving strong performance within their intended domains. However, these methods lack generalization across tasks. Although general-purpose restoration models (Chen et al. 2022a; Zamir et al. 2022) have been developed to handle multiple degradations, they often still

require separate models for each degradation type, resulting in complex inference and increased computational costs.

In recent years, All-in-One Image Restoration (AiOIR) methods (Wu et al. 2024a; Li et al. 2025a) have emerged as promising solutions. These frameworks can simultaneously handle diverse degradation types through various mechanisms. Early efforts, like AirNet (Li et al. 2022), focused on creating specific degradation encoders to capture distinctive feature representations. Subsequent innovations, such as those found in ProRes (Ma et al. 2023) and PromptIR (Potlapalli et al. 2023), enhanced performance by incorporating visual prompts. More recent research (Ai et al. 2024; Zhang et al. 2025c) has harnessed the powerful feature extraction capabilities of large-scale visual models to improve texture reconstruction and ensure structural integrity. However, these AiOIR methods overlook a critical issue: spatially non-uniform degradations can significantly alter the local statistical properties of an image. Most existing AiOIR approaches apply a uniform processing strategy across the entire image, failing to account for variations in degradation distribution and severity across different regions.

To address this limitation, as shown in Fig. 1, we design a progressive restoration pipeline inspired by Human Visual Perception (HVP), which refines image quality hierarchically from global structure to fine local details. First, as in early HVP stages, which emphasize global structure, we integrate an MLLM-based Image Quality Assessment (IQA) model to evaluate the image’s overall quality. Second, to better account for spatially varying degradation patterns, we incorporate a Semantic Guidance Unit (SGU) to support region-level segmentation and provide coarse guidance for identifying areas likely affected by degradation. Third, guided by the spatial cues from the SGU, we apply a task identifier to estimate the predominant degradation type in local neighborhoods. This allows ClearAIR to adaptively select region-appropriate restoration strategies, avoiding a uniform one-size-fits-all treatment across the image. Finally, to enhance the recovery of fine-grained local details, we propose an Internal Clue Reuse Mechanism (ICRM) that leverages internal image statistics to refine local structures.

Our main contributions can be summarized as follows:

- We present ClearAIR, a novel AiOIR framework inspired by HVP. By adopting a coarse-to-fine hierarchical restoration process, it gradually improves both structural

*Corresponding author.

Copyright © 2026, Association for the Advancement of Artificial Intelligence (www.aaai.org). All rights reserved.

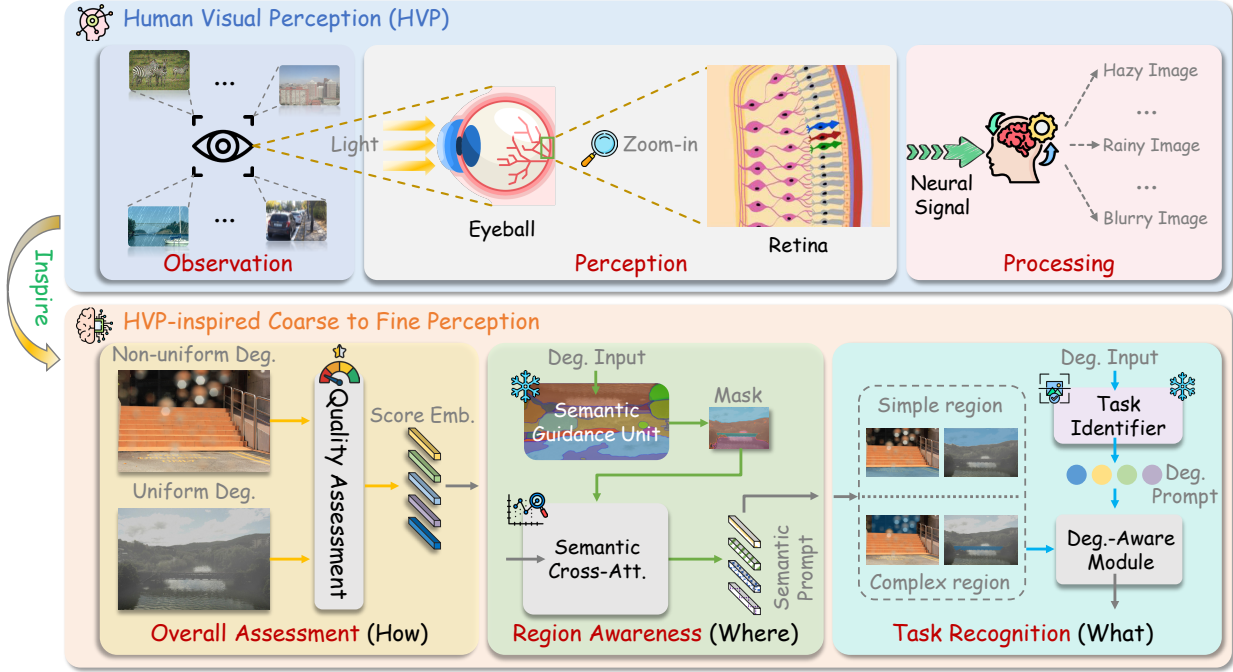


Figure 1: A coarse-to-fine image processing pipeline inspired by human visual perception.

integrity and perceptual quality.

- We propose an HVP-inspired pipeline integrating global quality and local semantic cues. An MLLM-based IQA evaluates quality, while the SGU and task identifier guide regional analysis and degradation estimation.
- We introduce ICRM that leverages self-supervised learning to exploit the intrinsic structure of the image, thereby enhancing the model’s ability to recover fine local details.

Related Work

All-in-One Image Restoration

All-in-One image restoration (Ma et al. 2025; Wu et al. 2025a; Zhang et al. 2025d; Wu et al. 2025b; Li et al. 2026) has emerged as a promising direction in low-level vision, aiming to restore clean images from diverse degradation types using a single unified model. Compared with task-specific (Zhang et al. 2023b; Li et al. 2025b; Cao et al. 2025; Li et al. 2024b; Xiao et al. 2024; Li et al. 2024d; Zhao et al. 2024; Li et al. 2024c; Xiao and Wang 2025; Chang et al. 2025a,b; Xiao et al. 2025b,a; Kong et al. 2023; Zhang et al. 2025b; Peng et al. 2025; Yang et al. 2025) and general restoration methods (Gou et al. 2020; Zhang et al. 2025a; Gou et al. 2024), all-in-one approaches offer significant advantages in multi-task capability, making it more suitable for practical applications with diverse degradation scenarios. For example, AirNet (Li et al. 2022) introduced a contrastive learning strategy to learn discriminative degradation representations. Prompt-based methods such as PromptIR (Potlapalli et al. 2023) and ProRes (Ma et al. 2023) further improved multi-degradation handling by incorporating vision

prompts into the network. More recently, DA-CLIP (Luo et al. 2023) and MPPerceiver (Ai et al. 2024) leveraged pre-trained large-scale vision models to boost performance on complex restoration tasks. Perceive-IR (Zhang et al. 2025c) showed that jointly recognizing degradation types and severity improves restoration, underscoring the importance of comprehensive degradation perception in all-in-one frameworks.

Despite these advancements, most all-in-one image restoration methods adopt a uniform processing strategy, failing to account for the spatial variability of degradation. Moreover, even in cases of uniformly distributed degradation, the difficulty of restoration varies significantly depending on the texture complexity of different regions. For example, flat regions are generally easier to restore, while areas with complex textures pose greater challenges.

Human Visual Perception

In visual cognition, humans exhibit specific characteristics. Typically, a visual image is first perceived as a unified whole before being analyzed in terms of its constituent parts. Recently, several studies have leveraged this perceptual mechanism to achieve promising results. For instance, Dream (Xia et al. 2024) reversely models the hierarchical processing of the Human Visual Perception (HVP) into a computable encoding-decoding framework, revealing that both biological and artificial vision systems aim for efficient visual information coding at their core. In this paper, we propose a hierarchical image perception pipeline that mimics human visual processing: global quality assessment to semantic-driven regional localization and degradation identification of distorted regions. By integrating global coarse-grained un-

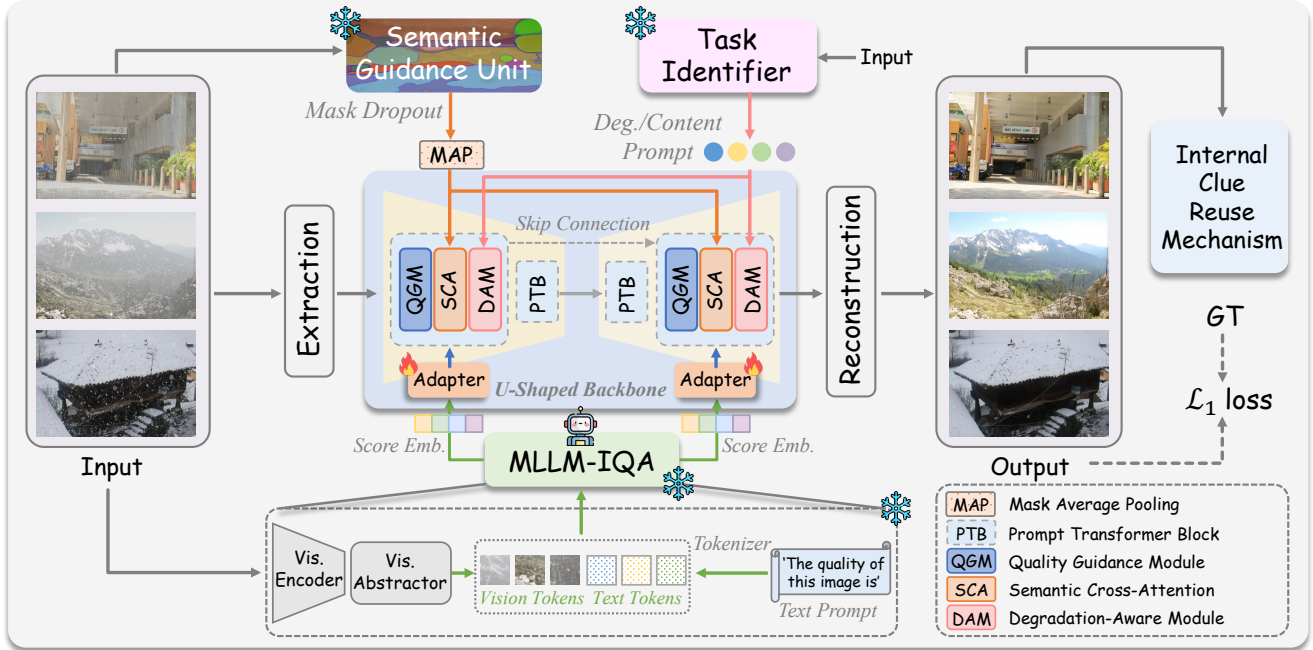


Figure 2: An overview architecture of the proposed ClearAIR.

derstanding and local fine-grained perception, our method not only improves the visual naturalness of restored images but also maintains semantic consistency under complex degradation, enabling more human-like AiOIR.

Image Quality Assessment

Image Quality Assessment (IQA) methods primarily rely on quality scores to evaluate image quality. These methods can be categorized into reference and no-reference approaches, depending on whether they require a high-quality reference image. In the field of image restoration, no-reference IQA is commonly used because it can directly regress a quality score without needing a reference image, aligning well with practical restoration needs. In recent years, Multi-Modal Large Language Models (MLLM)-based IQA methods have leveraged the foundational knowledge of MLLM to achieve superior performance and more detailed assessment results (Wu et al. 2024b,c). Q-Bench demonstrates that general MLLM possess some low-level perception capabilities. Q-Instruct further enhances these capabilities by introducing a large-scale dataset. Recently, DeQA (You et al. 2025) has advanced this area by using MLLM to regress precise quality scores, achieving remarkable performance. In this paper, we aim to harness the powerful ability of MLLMs to mine multi-modal cues, employing them as an initial estimator for overall image quality. This serves as a solid foundation for subsequent human visual perception processes.

Methodology

Overall Pipeline

The overall framework is illustrated in Fig. 2. ClearAIR consists of four components: 1) MLLM-based IQA: It gen-

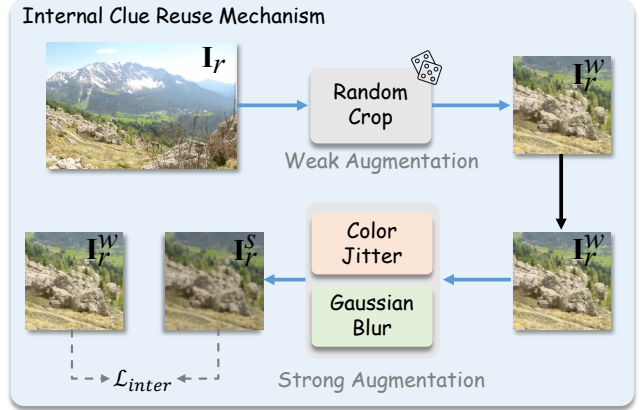


Figure 3: The proposed Internal Clue Reuse Mechanism.

erates a score embedding from visual and textual tokens, which guides the restoration backbone via the Quality Guidance Module (QGM). 2) Semantic Guidance Unit (SGU): It provides region-level semantic masks, with features fused through Semantic Cross-Attention (SCA). 3) Task Identifier: It estimates the predominant degradation type and encodes this prediction into a degradation prompt used by the Degradation-Aware Module (DAM). 4) Internal Clue Reuse Mechanism (ICRM): It exploits self-supervised learning to extract internal image cues, enhancing fine-detail reconstruction. The optimization objective of the overall process can be represented as:

$$\mathcal{L}_{total} = \mathcal{L}_1 + \alpha \cdot \mathcal{L}_{inter}, \quad (1)$$

where α is a hyperparameter set to 0.25. The details of \mathcal{L}_{inter} are provided in the ICRM subsection.

Overall Assessment. Inspired by the early HVP stages, which emphasize global structural cues, we incorporate an MLLM-IQA model to assess the overall quality of the input image. As shown in Fig. 2, a vision encoder is used to encode the input image into visual tokens. In addition, a vision abstractor is utilized as part of the connector module, which further compresses the visual tokens. Finally, the visual and textual tokens are fused and fed into a large MLLM for response prediction.

We extract the state \mathcal{Q} from the layer preceding the ‘quality level’ token. This representation more faithfully captures the MLLM-IQA model’s underlying reasoning about image quality. Subsequently, \mathcal{Q} is integrated into the QGM as score embeddings via an affine transformation. Given a degraded image \mathbf{I}_d along with its corresponding textual description \mathcal{T}_d , the above process can be expressed as follows:

$$\mathcal{Q} = \mathcal{M}_{iqa}(\mathbf{I}_d, \mathcal{T}_d), \quad (2)$$

$$\mathbf{F}_q = \mathcal{A}_{adpter}(\mathcal{Q}), \quad (3)$$

$$\mathbf{X}_{qgm}^{out} = \mathbf{X}_{qgm}^{in} \odot \text{Linear}(\mathbf{F}_q) + \text{Linear}(\mathbf{F}_q), \quad (4)$$

where $\mathcal{M}_{iqa}(\cdot)$ refers MLLM-based IQA model (DeQA). \mathbf{F}_q denotes the features after being transformed by the adapter \mathcal{A}_{adpter} . \mathbf{X}_{qgm}^{in} and \mathbf{X}_{qgm}^{out} represent the input and output features of the QGM, respectively.

Region Awareness. We design a region awareness pipeline to support region-level segmentation and provide coarse guidance for locating areas that are likely affected by degradation. Specifically, we introduce the SGU, which leverages a pre-trained Segment Anything Model (Ravi et al. 2024; Rong et al. 2025) to extract high-level semantics. Given a degraded image \mathbf{I}_d , SGU generates N_m binary masks:

$$\mathbf{I}_{mask} \in \{0, 1\}^{H \times W \times N_m}, \quad (5)$$

where each mask $m_i \in \mathbb{R}^{H \times W \times 1}$ highlights a distinct region. These masks are integrated with shallow features $\mathbf{F}_s \in \mathbb{R}^{H \times W \times C}$ via Mask Average Pooling (MAP). For each mask m_i , we compute the average feature within the masked region and broadcast it back:

$$\bar{\mathbf{f}}_i = \frac{1}{|\Omega_i|} \sum_{(h,w) \in \Omega_i} \mathbf{F}_s(h, w), \quad (6)$$

$$\mathbf{F}_{sem}(h, w) = \bar{\mathbf{f}}_i, \quad \forall (h, w) \in \Omega_i, \quad (7)$$

where $\Omega_i = \{(h, w) \mid m_i(h, w) = 1\}$. The output $\mathbf{F}_{sem} \in \mathbb{R}^{H \times W \times C}$ encodes semantic-aware structural priors.

To enhance robustness to fluctuations in mask quality resulting from degradation severity or model scale, we introduce mask dropout during training, removing a random subset of masks and merging their regions into the background. Finally, \mathbf{F}_{sem} interacts with the restoration backbone through SCA enabling region-level semantic guidance in the restoration process. This process can be expressed as follows:

$$\mathbf{Q} = \mathbf{F}_{sca}^{in}, \quad \mathbf{K} = \mathbf{W}_k \mathbf{F}_{sem}, \quad \mathbf{V} = \mathbf{W}_v \mathbf{F}_{sem}, \quad (8)$$

$$\mathbf{F}_{sca}^{out} = \text{Softmax} \left(\frac{\mathbf{Q} \mathbf{K}^T}{\sqrt{d}} \right) \mathbf{V}, \quad (9)$$

where \mathbf{F}_{sca}^{in} and \mathbf{F}_{sca}^{out} represent the input and output features of the SCA module, respectively.

Task Recognition. In this part, we primarily predict local degradation types, enabling a more informed characterization of region-level degradation patterns. Specifically, we employ DA-CLIP (Luo et al. 2023) as Task Identifier to generate both content embeddings $\mathbf{F}_c \in \mathbb{R}^{1 \times 512}$ and degradation embeddings $\mathbf{F}_d \in \mathbb{R}^{1 \times 512}$. The degradation embedding is then transformed into a degradation prompt \mathbf{F}_p , which can be described as:

$$\mathbf{F}_p = \text{MLP} \left(\mathcal{P} \odot \text{Softmax}(\text{MLP}(\mathbf{F}_d)) \right), \quad (10)$$

where \mathcal{P} denotes a set of learnable prompts. Subsequently, the feature \mathbf{X}_{dam}^{in} and \mathbf{F}_c are fed into the DAM, enabling cross-attention for content-aware spatial enhancement:

$$\hat{\mathbf{X}}_{dam}^{in} = \mathcal{C}_{1 \times 1}(\text{Norm}(\mathbf{X}_{dam}^{in})), \quad (11)$$

$$\mathbf{X}_{dam}^{att} = \text{CrossAtt.}(\mathbf{F}_c, \hat{\mathbf{X}}_{dam}^{in}). \quad (12)$$

Meanwhile, we generate a degradation mask $\mathbf{M}_d \in \mathbb{R}^{1 \times h \times w}$ based on \mathbf{F}_p , and then use \mathbf{F}_p to modulate the features $\hat{\mathbf{X}}_{dam}^{in}$. The process can be described as follows:

$$\mathbf{M}_d = \text{Sigmoid}(\text{MLP}(\mathbf{F}_p)), \quad (13)$$

$$\mathbf{F}_m = \mathbf{M}_d \odot \hat{\mathbf{X}}_{dam}^{in}, \quad (14)$$

where the modulated feature \mathbf{F}_m is concatenated with \mathbf{X}_{dam}^{att} and subsequently fused to get \mathbf{X}_{dam}^{out} .

Internal Clue Reuse Mechanism. As shown in Fig. 3, we introduce ICRM to enhance the model’s ability to preserve fine details in restored images. To achieve this, we apply data augmentation with different strengths to the restored output \mathbf{I}_r . First, weak augmentation is applied to \mathbf{I}_r , formulated as:

$$\mathbf{I}_r^w = \mathcal{F}_{weak}(\mathbf{I}_r), \quad (15)$$

where $\mathcal{F}_{weak}(\cdot)$ denotes a weak augmentation operation, and \mathbf{I}_r^w is the output image after applying $\mathcal{F}_{weak}(\cdot)$. Subsequently, strong augmentation is performed on the \mathbf{I}_r^w , which can be expressed as:

$$\mathbf{I}_r^s = \mathcal{F}_{strong}(\mathbf{I}_r^w), \quad (16)$$

where $\mathcal{F}_{strong}(\cdot)$ represents a strong augmentation operation, and \mathbf{I}_r^s is the resulting strongly augmented image. Finally, we compute the L2 distance between the weakly and strongly augmented results to form an internal consistency:

$$\mathcal{L}_{inter} = \gamma \cdot \|\mathbf{I}_r^w - \mathbf{I}_r^s\|_2^2, \quad (17)$$

where γ is a hyperparameter that controls the weight of this loss. In our experiments, we set the initial value of $\gamma = 0.05$.

Experiments

Experimental Setup

Datasets. We conduct experiments under two settings: All-in-One and Single-task following the protocols established in prior works (Zhang et al. 2025c). As shown in Tab. 1, the All-in-One setting entails a comprehensive evaluation across four tasks, with further details on the Single-task setting provided in the **Appendix**.

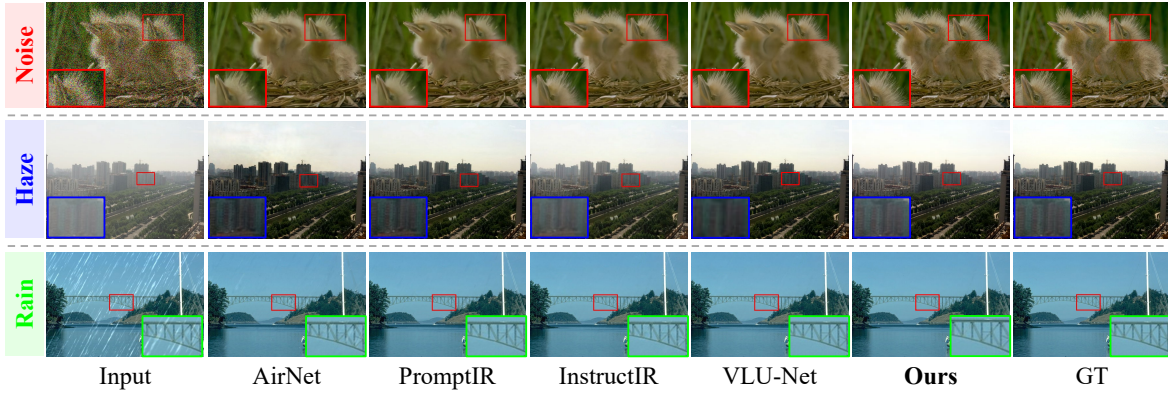


Figure 4: Visual comparisons of ClearAIR with state-of-the-art AiOIR methods on Three Degradations task.

Settings	No. Datasets	Degradation Type
Three Deg.	3	Noise, Haze, Rain
Five Deg.	5	Noise, Haze, Rain, Blur, Low-light
All-Weather	3	Haze, Rain, Raindrop, Snow
Composited Deg.	1	Haze, Rain, Low-light, Snow

Table 1: The details of the All-in-One setting.

Implementation Details. We employ DeQA (You et al. 2025) as the MLLM-IQA model and chose Restormer (Zamir et al. 2022) as the restoration backbone. Specifically, from level-1 to level-4, the numbers of Prompt Transformer Block (PTB) are set to [3, 5, 6, 8], the attention heads are [1, 2, 4, 8], and the channel dimensions are [48, 96, 192, 384]. We optimize the network using AdamW ($\beta_1 = 0.9$, $\beta_2 = 0.999$) with a learning rate of 2×10^{-4} and batch size of 4. Training runs for 300K iterations. The total loss weights are set as $\lambda_1 = 0.1$ and $\lambda_2 = 0.05$. All experiments are conducted on NVIDIA GeForce RTX 4090 GPUs. During training, inputs are randomly cropped to 256×256 patches, and random horizontal and vertical flips are applied for data augmentation.

All-in-One Image Restoration Results

Three Degradations Task. We evaluate our model on three restoration tasks: denoising, dehazing, and deraining. Tab. 2 shows ClearAIR achieves the best average performance, with notable improvements in high-noise removal and severe haze reduction. Outperforming or matching AdaIR and VLU-Net via better human visual perception modeling, it reaches 31.08 dB PSNR on SOTS (vs. 30.71 dB of VLU-Net), proving perceptual enhancement offsets the lack of physical priors. Qualitative results (Fig. 4) further verify its efficacy in texture preservation, rain streak removal with sharpness retention, and contrast/detail restoration in dense haze.

Five Degradations Task. We extend ClearAIR to five degradation tasks, using GoPro for deblurring and LOL for low-light enhancement. As shown in Tab. 3, ClearAIR achieves superior performance on most tasks, excelling par-

ticularly in deblurring. Although slightly behind specialized methods in low-light enhancement and denoising, it remains highly competitive and achieves the highest average PSNR (30.45 dB) and SSIM (0.916), demonstrating strong multi-task capability. Additional visual results are provided in the **Appendix**.

All-Weather Task. We evaluate ClearAIR on All-Weather task including: snow, rain & haze, and raindrop. Tab. 4 shows ClearAIR achieves an average gain of 0.22 dB over Histoformer (Sun et al. 2024). These consistent gains across diverse weather conditions demonstrate its effectiveness in handling complex adverse weather degradations. Qualitative comparisons in Fig. 5 further illustrate this: ClearAIR produces clearer, more natural results, effectively removing weather artifacts while better preserving details and textures.

Composited Degradation Task. We evaluate ClearAIR under challenging CDD-11 dataset (Guo et al. 2024), considering both individual and combined degradation. As shown in Tab. 5, ClearAIR achieves an average gain of 0.62 dB over OneRestore, outperforming existing All-in-One models, which validates its effectiveness in modeling human visual perception. Qualitative results in Fig. 6 demonstrate superior removal of composite degradations while preserving fine details and textures.

Ablation Study

This section analyzes the impact of different design choices in ClearAIR on model performance. All experiments are conducted on the Rain100L dataset (Yang et al. 2017) using a training of 100K iterations.

Effects of Perception Order. To investigate the impact of perception order, the sequence of overall assessment (How), region awareness and task Recognition (Where and What), we design two additional experimental setups based on the baseline order: Where-What-How and What-How-Where (indexes a and b). As shown in Tab. 6, the Where-What-How order yields the worst performance. This may be because perceiving region-level semantic information first disrupts the structural integrity that is crucial for coarse quality assessment. Notably, the What-How-Where order achieves

Method	Source	Params.	Dehazing		Deraining		Denoising		Average					
			SOTS	Rain100L	BSD68 $_{\sigma=15}$	BSD68 $_{\sigma=25}$	BSD68 $_{\sigma=50}$							
DL (Fan et al. 2019)	TPAMI’19	2M	26.92	.931	32.62	.931	33.05	.914	30.41	.861	26.90	.740	29.98	.876
AirNet (Li et al. 2022)	CVPR’22	9M	27.94	.962	34.90	.967	33.92	.933	31.26	.888	28.00	.797	31.20	.910
IDR (Zhang et al. 2023a)	CVPR’23	15M	29.87	.970	36.03	.971	33.89	.931	31.32	.884	28.04	.798	31.83	.911
PromptIR (Potlapalli et al. 2023)	NeurIPS’23	36M	30.58	.974	36.37	.972	33.98	.933	31.31	.888	28.06	.799	32.06	.913
NDR (Yao et al. 2024)	TIP’24	28M	28.64	.962	35.42	.969	34.01	.932	31.36	.887	28.10	.798	31.51	.910
Gridformer (Wang et al. 2024)	IJCV’24	34M	30.37	.970	37.15	.972	33.93	.931	31.37	.887	28.11	.801	32.19	.912
InstructIR (Conde, Geigle, and Timofte 2024)	ECCV’24	16M	30.22	.959	37.98	.978	34.15	.933	31.52	.890	28.30	.803	32.43	.913
Perceive-IR (Zhang et al. 2025c)	TIP’25	42M	30.87	.975	38.29	.980	34.13	.934	31.53	.890	28.31	.804	32.63	.917
AdaIR (Cui et al. 2025)	ICLR’25	29M	31.06	.980	38.64	.983	34.12	.934	31.45	.892	28.19	.802	32.69	.918
VLU-Net (Zeng et al. 2025)	CVPR’25	35M	30.71	.980	38.93	.984	34.13	.935	31.48	.892	28.23	.804	32.70	.919
ClearAIR (Ours)	-	31M	31.08	.981	38.61	.984	34.18	.935	31.50	<u>.891</u>	28.31	.804	32.74	.919

Table 2: Comparison to state-of-the-art AiOIR methods on Three Degradations task.

Method	Source	Params.	Dehazing		Deraining		Denoising		Deblurring		Low-Light		Average	
			SOTS	Rain100L	BSD68 $_{\sigma=25}$	GoPro	LOLv1							
DL (Fan et al. 2019)	TPAMI’19	2M	20.54	.826	21.96	.762	23.09	.745	19.86	.672	19.83	.712	21.05	.743
AirNet (Li et al. 2022)	CVPR’22	9M	21.04	.884	32.98	.951	30.91	.882	24.35	.781	18.18	.735	25.49	.847
IDR (Zhang et al. 2023a)	CVPR’23	15M	25.24	.943	35.63	.965	31.60	.887	27.87	.846	21.34	.826	28.34	.893
PromptIR (Potlapalli et al. 2023)	NeurIPS’23	33M	26.54	.949	36.37	.970	31.47	.886	28.71	.881	22.68	.832	29.15	.904
Gridformer (Wang et al. 2024)	IJCV’24	34M	26.79	.951	36.61	.971	31.45	.885	29.22	.884	22.59	.831	29.33	.904
InstructIR (Conde, Geigle, and Timofte 2024)	ECCV’24	16M	27.10	.956	36.84	.973	31.40	.887	29.40	.886	23.00	.836	29.55	.907
Perceive-IR (Zhang et al. 2025c)	TIP’25	42M	28.19	.964	37.25	.977	31.44	.887	29.46	.886	22.81	.833	29.84	.909
AdaIR (Cui et al. 2025)	ICLR’25	29M	30.53	.978	38.02	.981	31.35	.888	28.12	.858	23.00	.845	30.20	.910
VLU-Net (Zeng et al. 2025)	CVPR’25	35M	30.84	.980	38.54	.982	31.43	.891	27.46	.840	22.29	.833	30.11	.905
ClearAIR (Ours)	-	31M	30.12	.978	38.20	.982	31.53	.888	29.67	.887	22.83	.846	30.45	.916

Table 3: Comparison to state-of-the-art AiOIR methods on Five Degradations task.

Method	Source	Params.	Snow100K-S				Snow100K-L				Outdoor-Rain		RainDrop		Average
			PSNR	SSIM	PSNR	SSIM									
All-in-One (Li, Tan, and Cheong 2020)	CVPR’20	-	-	-	28.33	.882	24.71	.898	31.12	.927	28.05	.902			
Transweather (Valanarasu, Yasarla, and Patel 2022)	CVPR’22	38M	32.51	.934	29.31	.888	28.83	.900	30.17	.916	30.20	.909			
TKL (Chen et al. 2022b)	CVPR’22	29M	34.42	.947	30.22	.907	29.27	.915	31.81	.931	31.43	.925			
WGWSNet (Zhu et al. 2023)	CVPR’23	26M	34.31	.946	30.16	.901	29.32	.921	32.38	.938	31.54	.926			
WeatherDiff (Özdenizci and Legenstein 2023)	TPAMI’23	83M	35.83	.957	30.09	.904	29.64	.931	30.71	.931	31.57	.931			
AWRCP (Ye et al. 2023)	ICCV’23	-	36.92	.965	31.92	.934	31.39	.933	31.93	.931	33.04	.941			
Histoformer (Sun et al. 2024)	ECCV’24	30M	37.41	.966	32.16	.926	32.08	.939	33.06	.944	33.68	.945			
T ³ -DiffWeather (Chen et al. 2024)	ECCV’24	69M	<u>37.51</u>	.966	<u>32.37</u>	.936	31.09	.937	32.66	.941	33.41	.945			
ClearAIR (Ours)	-	31M	37.79	.967	32.53	<u>.932</u>	32.45	.941	32.82	<u>.942</u>	33.90	.946			

Table 4: Comparison to state-of-the-art All-in-One methods on All-Weather task.

the second-best result, which aligns with the workflow of some AiOIR methods that begin with degradation characterization. In contrast, our method, inspired by the human visual perception process, achieves the best overall performance.

Effects of Different Components

As shown in Tab. 7, we conduct ablation studies to evaluate the contribution of each proposed component. The experimental settings are as follows: (1) w/o MLLM-IQA (IQA): replaces quality guidance with a learnable parame-

ter; (2) w/o SGU: replaces semantic priors with learnable parameters; (3) w/o Task identifier (TI): removes degradation prompts, using a learnable parameter instead; (4) w/o LCRM: removes the Internal Clue Reuse Mechanism. Variants (a–c), which replace structured priors with unstructured learnable parameters, exhibit clear performance degradation, demonstrating the necessity of explicit prior modeling for reliable guidance and task adaptation. Variants (d–f), which preserve partial structured cues (e.g., quality or degradation estimation), yield noticeable improvements, underscoring the value of perceptual and degradation awareness.

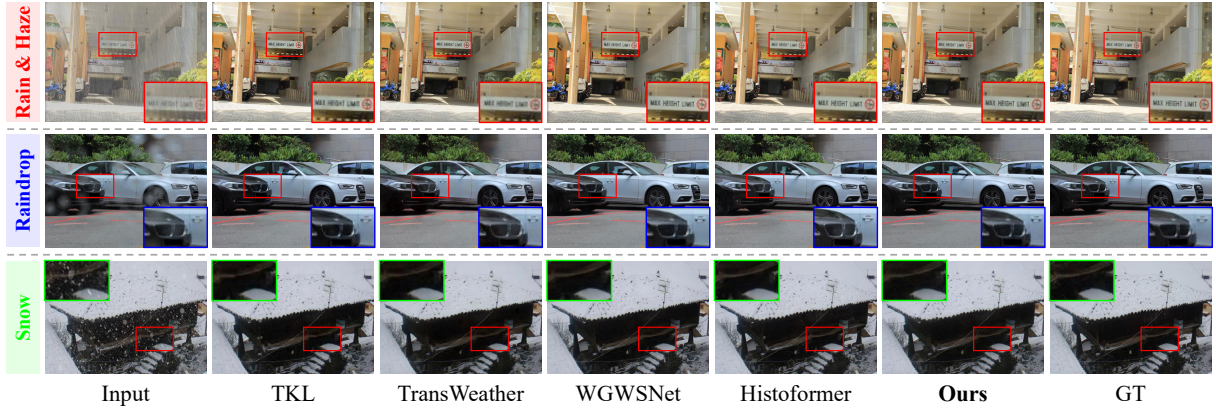


Figure 5: Visual comparisons of ClearAIR with state-of-the-art AiOIR methods on All-Weather task.

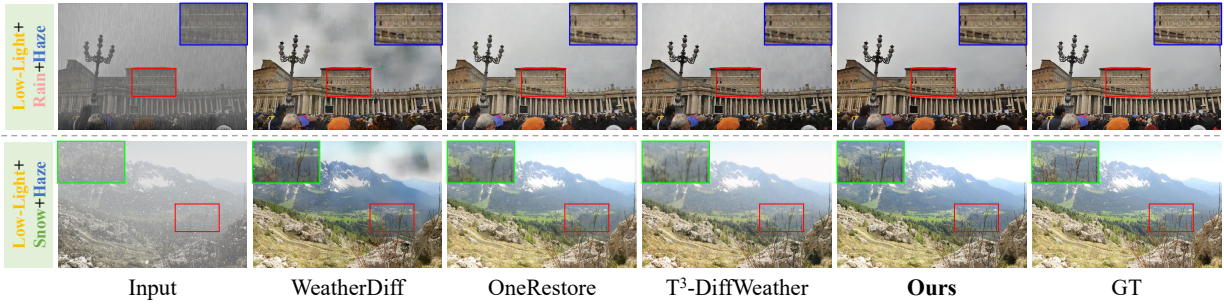


Figure 6: Visual comparisons of ClearAIR with state-of-the-art AiOIR methods on Composited Degradation task.

Method	Source	Params.	PSNR↑	SSIM↑
AirNet	CVPR'22	9M	23.75	0.814
TransWeather	CVPR'22	38M	23.13	0.781
WeatherDiff	TPAMI'23	83M	22.49	0.799
PromptIR	NeurIPS'23	33M	25.90	0.850
WGWSNet	CVPR'23	26M	26.96	0.863
OneRestore	ECCV'24	6M	28.72	0.882
ClearAIR (Ours)	-	31M	29.34	0.886

Table 5: Comparison to state-of-the-art All-in-One methods on Composited Degradations task (CDD-11 dataset).

Index	Order	PSNR↑	SSIM↑
a	Where-What-How	37.89	0.982
b	What-How-Where	38.04	0.983
Ours	How-Where-What	38.21	0.986

Table 6: Effectiveness of perception order.

Removing LCRM (g) also reduces performance, though to a lesser extent, indicating its benefit in leveraging internal structures and contextual information.

Conclusion

In this paper, we propose ClearAIR, a novel AiOIR framework inspired by HVP and designed with a hierarchical,

Index	IQA	SGU	TI	ICRM	PSNR↑	SSIM↑
a	✓	✗	✗	✓	37.57	0.980
b	✗	✓	✗	✓	37.43	0.978
c	✗	✗	✓	✓	37.52	0.980
d	✓	✓	✗	✓	38.05	0.985
e	✓	✗	✓	✓	37.93	0.984
f	✗	✓	✓	✓	37.87	0.984
g	✓	✓	✓	✗	38.03	0.985
Ours	✓	✓	✓	✓	38.21	0.986

Table 7: Effectiveness of different components.

coarse-to-fine restoration strategy. By mimicking the HVP's tendency to first perceive an image as a whole before focusing on local details, our method integrates overall assessment, region awareness, task Recognition, and internal clue reuse mechanism for fine-grained restoration. The combination of an MLLM-based image quality assessment model, the semantic guidance unit, and a task identifier enables accurate localization and understanding of degradation patterns. Furthermore, the proposed internal clue reuse mechanism enhances the model's ability to recover detailed textures in a self-supervised manner. Experimental results demonstrate that ClearAIR achieves state-of-the-art performance on both synthetic and real-world datasets.

Acknowledgments

This work was supported by the National Natural Science Foundation of China under Grant 62431020, the National Key Research and Development Program of China under Grant 2024YFE0111800, and the Fundamental Research Funds for the Central Universities under Grant 2042025kf0030.

References

Agustsson, E.; and Timofte, R. 2017. Ntire 2017 challenge on single image super-resolution: Dataset and study. In *CVPRW*, 126–135.

Ai, Y.; Huang, H.; Zhou, X.; Wang, J.; and He, R. 2024. Multimodal prompt perceiver: Empower adaptiveness generalizability and fidelity for all-in-one image restoration. In *CVPR*, 25432–25444.

Arbelaez, P.; Maire, M.; Fowlkes, C.; and Malik, J. 2010. Contour detection and hierarchical image segmentation. *IEEE TPAMI*, 33(5): 898–916.

Cai, B.; Xu, X.; Jia, K.; Qing, C.; and Tao, D. 2016. Dehazenet: An end-to-end system for single image haze removal. *IEEE TIP*, 25(11): 5187–5198.

Cao, J.; Zeng, Z.; Zhang, X.; Zhang, H.; Fan, C.; Jiang, G.; and Lin, W. 2025. Unveiling the underwater world: CLIP perception model-guided underwater image enhancement. *PR*, 162: 111395.

Chang, L.; Wang, Y.; Deng, L.; Du, B.; and Xu, C. 2025a. WaterDiffusion: Learning a Prior-involved Unrolling Diffusion for Joint Underwater Saliency Detection and Visual Restoration. In *AAAI*, 1998–2006.

Chang, L.; Wang, Y.; Du, B.; and Xu, C. 2025b. Color Correction Meets Cross-Spectral Refinement: A Distribution-Aware Diffusion for Underwater Image Restoration. *arXiv preprint arXiv:2501.04740*.

Chen, L.; Chu, X.; Zhang, X.; and Sun, J. 2022a. Simple baselines for image restoration. In *ECCV*, 17–33.

Chen, S.; Ye, T.; Zhang, K.; Xing, Z.; Lin, Y.; and Zhu, L. 2024. Teaching Tailored to Talent: Adverse Weather Restoration via Prompt Pool and Depth-Anything Constraint. In *ECCV*, 95–115.

Chen, W.-T.; Huang, Z.-K.; Tsai, C.-C.; Yang, H.-H.; Ding, J.-J.; and Kuo, S.-Y. 2022b. Learning multiple adverse weather removal via two-stage knowledge learning and multi-contrastive regularization: Toward a unified model. In *CVPR*, 17653–17662.

Chen, X.; Li, H.; Li, M.; and Pan, J. 2023. Learning a Sparse Transformer Network for Effective Image Deraining. In *CVPR*, 5896–5905.

Chou, C.-H.; and Li, Y.-C. 1995. A perceptually tuned subband image coder based on the measure of just-noticeable-distortion profile. *IEEE TCSVT*, 5(6): 467–476.

Conde, M. V.; Geigle, G.; and Timofte, R. 2024. High-quality image restoration following human instructions. In *ECCV*, 1–21.

Cui, Y.; Ren, W.; Cao, X.; and Knoll, A. 2023. Image restoration via frequency selection. *IEEE TPAMI*, 46(2): 1093–1108.

Cui, Y.; Zamir, S. W.; Khan, S.; Knoll, A.; Shah, M.; and Khan, F. S. 2025. Adair: Adaptive all-in-one image restoration via frequency mining and modulation. In *ICLR*, 57335–57356.

Fan, Q.; Chen, D.; Yuan, L.; Hua, G.; Yu, N.; and Chen, B. 2019. A general decoupled learning framework for parameterized image operators. *IEEE TPAMI*, 43(1): 33–47.

Franzen, R. 1999. Kodak lossless true color image suite. [Online]. Available: <http://r0k.us/graphics/kodak/>. [Accessed: Oct. 24, 2021].

Gou, Y.; Li, B.; Liu, Z.; Yang, S.; and Peng, X. 2020. Clearer: Multi-scale neural architecture search for image restoration. In *NeurIPS*, 17129–17140.

Gou, Y.; Zhao, H.; Li, B.; Xiao, X.; and Peng, X. 2024. Test-Time Degradation Adaptation for Open-Set Image Restoration. In *ICML*, 16167–16177.

Guo, Y.; Gao, Y.; Lu, Y.; Zhu, H.; Liu, R. W.; and He, S. 2024. Onerestore: A universal restoration framework for composite degradation. In *ECCV*, 255–272.

Huang, J.-B.; Singh, A.; and Ahuja, N. 2015. Single image super-resolution from transformed self-exemplars. In *CVPR*, 5197–5206.

Jiang, K.; Wang, Z.; Yi, P.; Chen, C.; Huang, B.; Luo, Y.; Ma, J.; and Jiang, J. 2020. Multi-scale progressive fusion network for single image deraining. In *CVPR*, 8346–8355.

Ke, J.; Wang, Q.; Wang, Y.; Milanfar, P.; and Yang, F. 2021. Musiq: Multi-scale image quality transformer. In *ICCV*, 5148–5157.

Kong, L.; Dong, J.; Ge, J.; Li, M.; and Pan, J. 2023. Efficient frequency domain-based transformers for high-quality image deblurring. In *CVPR*, 5886–5895.

Li, B.; Liu, X.; Hu, P.; Wu, Z.; Lv, J.; and Peng, X. 2022. All-in-one image restoration for unknown corruption. In *CVPR*, 17452–17462.

Li, B.; Peng, X.; Wang, Z.; Xu, J.; and Feng, D. 2017. Aodnet: All-in-one dehazing network. In *ICCV*, 4770–4778.

Li, B.; Ren, W.; Fu, D.; Tao, D.; Feng, D.; Zeng, W.; and Wang, Z. 2018. Benchmarking single-image dehazing and beyond. *IEEE TIP*, 28(1): 492–505.

Li, H.; Chen, X.; Dong, J.; Tang, J.; and Pan, J. 2025a. Foundir: Unleashing million-scale training data to advance foundation models for image restoration. In *ICCV*, 12626–12636.

Li, R.; Cheong, L.-F.; and Tan, R. T. 2019. Heavy rain image restoration: Integrating physics model and conditional adversarial learning. In *CVPR*, 1633–1642.

Li, R.; Tan, R. T.; and Cheong, L.-F. 2020. All in one bad weather removal using architectural search. In *CVPR*, 3175–3185.

Li, S.; Liu, M.; Zhang, Y.; Chen, S.; Li, H.; Dou, Z.; and Chen, H. 2024a. Sam-deblur: Let segment anything boost image deblurring. In *ICASSP*, 2445–2449.

Li, W.; Chen, H.; Xiao, Y.; Zuo, W.; Zhou, J.; Tian, Y.; and Fan, X. 2026. All-in-One Video Restoration under Smoothly Evolving Unknown Weather Degradations. *arXiv preprint arXiv:2601.00533*.

Li, W.; Han, W.; Deng, L.-J.; Xiong, R.; and Fan, X. 2025b. Spiking Variational Graph Representation Inference for Video Summarization. *IEEE TIP*, 34: 5697–5709.

Li, W.; Wang, P.; Xiong, R.; and Fan, X. 2024b. Spiking Tucker Fusion Transformer for Audio-Visual Zero-Shot Learning. *IEEE TIP*, 33: 4840–4852.

Li, Z.; Li, J.; Li, Y.; Li, L.; Liu, D.; and Wu, F. 2024c. In-loop filtering via trained look-up tables. In *VCIP*, 1–5.

Li, Z.; Yuan, Z.; Li, L.; Liu, D.; Tang, X.; and Wu, F. 2024d. Object Segmentation-Assisted Inter Prediction for Versatile Video Coding. *IEEE TBC*, 70(4): 1236–1253.

Liu, L.; Xie, L.; Zhang, X.; Yuan, S.; Chen, X.; Zhou, W.; Li, H.; and Tian, Q. 2022. Tape: Task-agnostic prior embedding for image restoration. In *ECCV*, 447–464.

Liu, Y.-F.; Jaw, D.-W.; Huang, S.-C.; and Hwang, J.-N. 2018. Desnownet: Context-aware deep network for snow removal. *IEEE TIP*, 27(6): 3064–3073.

Luo, Z.; Gustafsson, F. K.; Zhao, Z.; Sjölund, J.; and Schön, T. B. 2023. Controlling vision-language models for universal image restoration. In *ICLR*, 16226–16246.

Ma, J.; Cheng, T.; Wang, G.; Zhang, Q.; Wang, X.; and Zhang, L. 2023. ProRes: Exploring Degradation-aware Visual Prompt for Universal Image Restoration. *arXiv preprint arXiv:2306.13653*.

Ma, J.; Hu, S.; Zhang, X.; Wan, J.; Huang, J.; Zhang, L.; and Khan, S. 2025. EvoIR: Towards All-in-One Image Restoration via Evolutionary Frequency Modulation. *arXiv preprint arXiv:2512.05104*.

Ma, K.; Duanmu, Z.; Wu, Q.; Wang, Z.; Yong, H.; Li, H.; and Zhang, L. 2016. Waterloo exploration database: New challenges for image quality assessment models. *IEEE TIP*, 26(2): 1004–1016.

Martin, D.; Fowlkes, C.; Tal, D.; and Malik, J. 2001. A database of human segmented natural images and its application to evaluating segmentation algorithms and measuring ecological statistics. In *ICCV*, 416–423.

Mittal, A.; Soundararajan, R.; and Bovik, A. C. 2012. Making a “completely blind” image quality analyzer. *IEEE SPL*, 20(3): 209–212.

Mou, C.; Wang, Q.; and Zhang, J. 2022. Deep generalized unfolding networks for image restoration. In *CVPR*, 17399–17410.

Nah, S.; Hyun Kim, T.; and Mu Lee, K. 2017. Deep multi-scale convolutional neural network for dynamic scene deblurring. In *CVPR*, 3883–3891.

Özdenizci, O.; and Legenstein, R. 2023. Restoring vision in adverse weather conditions with patch-based denoising diffusion models. *IEEE TPAMI*, 45(8): 10346–10357.

Peng, L.; Wu, A.; Li, W.; Xia, P.; Dai, X.; Zhang, X.; Di, X.; Sun, H.; Pei, R.; Wang, Y.; et al. 2025. Pixel to gaussian: Ultra-fast continuous super-resolution with 2d gaussian modeling. *arXiv preprint arXiv:2503.06617*.

Potlapalli, V.; Zamir, S. W.; Khan, S.; and Khan, F. S. 2023. PromptIR: Prompting for All-in-One Blind Image Restoration. In *NeurIPS*, 71275–71293.

Qian, R.; Tan, R. T.; Yang, W.; Su, J.; and Liu, J. 2018. Attentive generative adversarial network for raindrop removal from a single image. In *CVPR*, 2482–2491.

Quan, R.; Yu, X.; Liang, Y.; and Yang, Y. 2021. Removing raindrops and rain streaks in one go. In *CVPR*, 9147–9156.

Ravi, N.; Gabeur, V.; Hu, Y.-T.; Hu, R.; Ryali, C.; Ma, T.; Khedr, H.; Rädle, R.; Rolland, C.; Gustafson, L.; et al. 2024. Sam 2: Segment anything in images and videos. *arXiv preprint arXiv:2408.00714*.

Rong, F.; Lan, M.; Zhang, Q.; and Zhang, L. 2025. MPG-SAM 2: Adapting SAM 2 with Mask Priors and Global Context for Referring Video Object Segmentation. *arXiv preprint arXiv:2501.13667*.

Shen, H.; Zhao, Z.-Q.; and Zhang, W. 2023. Adaptive dynamic filtering network for image denoising. In *AAAI*, 2227–2235.

Shi, Y.; Weng, Z.; Lin, Y.; Shi, C.; Guo, X.; Yang, X.; and Lin, L. 2025. Scaling Up Single Image Dehazing Algorithm by Cross-Data Vision Alignment for Richer Representation Learning and Beyond. *IEEE TIM*, 74: 1–9.

Song, Y.; He, Z.; Qian, H.; and Du, X. 2023. Vision Transformers for Single Image Dehazing. *IEEE TIP*, 32: 1927–1941.

Sun, S.; Ren, W.; Gao, X.; Wang, R.; and Cao, X. 2024. Restoring images in adverse weather conditions via histogram transformer. In *ECCV*, 111–129.

Valanarasu, J. M. J.; Yasarla, R.; and Patel, V. M. 2022. Transweather: Transformer-based restoration of images degraded by adverse weather conditions. In *CVPR*, 2353–2363.

Wang, T.; Zhang, K.; Shao, Z.; Luo, W.; Stenger, B.; Lu, T.; Kim, T.-K.; Liu, W.; and Li, H. 2024. Gridformer: Residual dense transformer with grid structure for image restoration in adverse weather conditions. *IJCV*, 132(10): 4541–4563.

Wang, Z.; Bovik, A. C.; Sheikh, H. R.; and Simoncelli, E. P. 2004. Image quality assessment: from error visibility to structural similarity. *IEEE TIP*, 13(4): 600–612.

Wei, C.; Wang, W.; Yang, W.; and Liu, J. 2018. Deep retinex decomposition for low-light enhancement. In *BMVC*.

Wu, G.; Jiang, J.; Jiang, K.; and Liu, X. 2024a. Learning from history: Task-agnostic model contrastive learning for image restoration. In *AAAI*, 5976–5984.

Wu, G.; Jiang, J.; Jiang, K.; Liu, X.; and Nie, L. 2025a. Learning Dynamic Prompts for All-in-One Image Restoration. *IEEE TIP*, 34: 3997–4010.

Wu, G.; Jiang, J.; Wang, Y.; Jiang, K.; and Liu, X. 2025b. Debiased All-in-one Image Restoration with Task Uncertainty Regularization. In *AAAI*, 8386–8394.

Wu, H.; Zhang, Z.; Zhang, E.; Chen, C.; Liao, L.; Wang, A.; Li, C.; Sun, W.; Yan, Q.; Zhai, G.; et al. 2024b. Q-bench: A benchmark for general-purpose foundation models on low-level vision. In *ICLR*, 12547–12573.

Wu, H.; Zhang, Z.; Zhang, E.; Chen, C.; Liao, L.; Wang, A.; Xu, K.; Li, C.; Hou, J.; Zhai, G.; et al. 2024c. Q-instruct: Improving low-level visual abilities for multi-modality foundation models. In *CVPR*, 25490–25500.

Xia, W.; De Charette, R.; Oztireli, C.; and Xue, J.-H. 2024. Dream: Visual decoding from reversing human visual system. In *WACV*, 8226–8235.

Xiao, Y.; Yuan, Q.; Jiang, K.; Chen, Y.; Wang, S.; and Lin, C.-W. 2025a. Multi-Axis Feature Diversity Enhancement for Remote Sensing Video Super-Resolution. *IEEE TIP*, 34: 1766–1778.

Xiao, Y.; Yuan, Q.; Jiang, K.; Huang, W.; Zhang, Q.; Zheng, T.; Lin, C.-W.; and Zhang, L. 2025b. Spiking Meets Attention: Efficient Remote Sensing Image Super-Resolution with Attention Spiking Neural Networks. *arXiv preprint arXiv:2503.04223*.

Xiao, Z.; Kai, D.; Zhang, Y.; Zha, Z.-J.; Sun, X.; and Xiong, Z. 2024. Event-adapted video super-resolution. In *ECCV*, 217–235.

Xiao, Z.; and Wang, X. 2025. Event-based Video Super-Resolution via State Space Models. In *CVPR*, 12564–12574.

Yang, H.; Zhang, X.; Ma, J.; Zhu, L.; Zhang, Y.; and Zhang, H. 2025. Hierarchical graph attention network for no-reference omnidirectional image quality assessment. *arXiv preprint arXiv:2508.09843*.

Yang, W.; Tan, R. T.; Feng, J.; Liu, J.; Guo, Z.; and Yan, S. 2017. Deep joint rain detection and removal from a single image. In *CVPR*, 1357–1366.

Yao, M.; Xu, R.; Guan, Y.; Huang, J.; and Xiong, Z. 2024. Neural Degradation Representation Learning for All-in-One Image Restoration. *IEEE TIP*, 33: 5408–5423.

Yasarla, R.; and Patel, V. M. 2019. Uncertainty guided multi-scale residual learning-using a cycle spinning cnn for single image de-raining. In *CVPR*, 8405–8414.

Ye, T.; Chen, S.; Bai, J.; Shi, J.; Xue, C.; Jiang, J.; Yin, J.; Chen, E.; and Liu, Y. 2023. Adverse weather removal with codebook priors. In *ICCV*, 12653–12664.

You, Z.; Cai, X.; Gu, J.; Xue, T.; and Dong, C. 2025. Teaching large language models to regress accurate image quality scores using score distribution. In *CVPR*, 14483–14494.

Zamir, S. W.; Arora, A.; Khan, S.; Hayat, M.; Khan, F. S.; and Yang, M.-H. 2022. Restormer: Efficient transformer for high-resolution image restoration. In *CVPR*, 5728–5739.

Zeng, H.; Wang, X.; Chen, Y.; Su, J.; and Liu, J. 2025. Vision-Language Gradient Descent-driven All-in-One Deep Unfolding Networks. In *CVPR*, 7524–7533.

Zhang, H.; Zhang, X.; Cai, N.; Di, J.; and Zhang, Y. 2025a. Joint multi-dimensional dynamic attention and transformer for general image restoration. *CVIU*, 261: 104491.

Zhang, H.; Zhang, X.; Zhu, L.; Zhang, Y.; Cao, J.; and Ling, W.-K. 2025b. Enhancing 3D video watching experiences: Tackling compression and 3D warping distortions in synthesized view with perceptual guidance. *ESWA*, 264: 125853.

Zhang, J.; Huang, J.; Yao, M.; Yang, Z.; Yu, H.; Zhou, M.; and Zhao, F. 2023a. Ingredient-Oriented Multi-Degradation Learning for Image Restoration. In *CVPR*, 5825–5835.

Zhang, K.; Zuo, W.; Chen, Y.; Meng, D.; and Zhang, L. 2017. Beyond a gaussian denoiser: Residual learning of deep cnn for image denoising. *IEEE TIP*, 26(7): 3142–3155.

Zhang, K.; Zuo, W.; and Zhang, L. 2018. FFDNet: Toward a fast and flexible solution for CNN-based image denoising. *IEEE TIP*, 27(9): 4608–4622.

Zhang, X.; Cai, N.; Zhang, H.; Zhang, Y.; Di, J.; and Lin, W. 2023b. AFD-Former: A Hybrid Transformer With Asymmetric Flow Division for Synthesized View Quality Enhancement. *IEEE TCSVT*, 33(8): 3786–3798.

Zhang, X.; Ma, J.; Wang, G.; Zhang, Q.; Zhang, H.; and Zhang, L. 2025c. Perceive-ir: Learning to perceive degradation better for all-in-one image restoration. *IEEE TIP*.

Zhang, X.; Zhang, H.; Wang, G.; Zhang, Q.; Zhang, L.; and Du, B. 2025d. UniUIR: Considering Underwater Image Restoration as an All-in-One Learner. *IEEE TIP*, 34: 6963–6977.

Zhao, R.; Xiong, R.; Zhao, J.; Zhang, J.; Fan, X.; Yu, Z.; and Huang, T. 2024. Boosting spike camera image reconstruction from a perspective of dealing with spike fluctuations. In *CVPR*, 24955–24965.

Zhu, Y.; Wang, T.; Fu, X.; Yang, X.; Guo, X.; Dai, J.; Qiao, Y.; and Hu, X. 2023. Learning Weather-General and Weather-Specific Features for Image Restoration Under Multiple Adverse Weather Conditions. In *CVPR*, 21747–21758.

Supplementary Material

Appendix

A. More Details on Datasets and Evaluation

Datasets. Following (Zhang et al. 2025c, 2023a), we categorize training setups into “All-in-One” and “Single-task” based on whether datasets are combined for mixed training. For AiOIR, we train on a mixed dataset containing multiple degradations and test one by one on the dataset containing a single type of degradation. Four All-in-One settings are summarized as follows, each specifying the included degradation types and corresponding datasets:

- **Three Degradations:** Gaussian noise (using BSD400 (Arbelaez et al. 2010), WED (Ma et al. 2016), and BSD68 (Martin et al. 2001)), haze (SOTS (Li et al. 2018)), and rain (Rain100L (Yang et al. 2017)).
- **Five Degradations:** Extends the Three Degradations setting by adding Motion Blur (GoPro (Nah, Hyun Kim, and Mu Lee 2017)) and Low-light (LOL (Wei et al. 2018)).
- **All-Weather:** Focuses on adverse weather conditions: Haze & Rain (Outdoor-Rain (Li, Cheong, and Tan 2019)), Raindrop (Raindrop (Qian et al. 2018)), and Snow (Snow100K (Liu et al. 2018)).
- **Composed Degradations:** A challenging combinations of Haze, Rain, Low-light, and Snow is synthesized on the DIV2K dataset (Agustsson and Timofte 2017) and is known as the CDD-11 benchmark (Guo et al. 2024).

Under the “Single-task” setting, the model is trained and tested on one specific restoration task at a time. The datasets used for each task are detailed below:

- **Image Denoising:** Training is performed on a merged dataset of BSD400 (400 images) and WED (4,744 images). Noisy images are generated by adding Gaussian noise with levels $\sigma \in \{15, 25, 50\}$. Testing is conducted on the BSD68, Urban100 (Huang, Singh, and Ahuja 2015), and Kodak24 (Franzen 1999) datasets.
- **Image Dehazing:** The OTS subset of RESIDE- β (Li et al. 2018) (72,135 pairs) is used for training, and the SOTS-Outdoor dataset (Li et al. 2018) (500 images) for testing.
- **Image Deraining:** The Rain100L dataset is used, with 200 image pairs for training and 100 pairs for testing.

Evaluation Metrics. We assess model performance using both reference-based and no-reference image quality metrics. The former includes Peak Signal-to-Noise Ratio (PSNR) and Structural Similarity Index (SSIM) (Wang et al. 2004), while the latter comprises the Multi-scale Image Quality Transformer (MUSIQ) (Ke et al. 2021) and the Natural Image Quality Evaluator (NIQE) (Mittal, Soundararajan, and Bovik 2012). Higher values of PSNR, SSIM, and MUSIQ indicate better quality, whereas lower NIQE scores correspond to superior perceptual quality.

B. More Experiment Results

Generalization to Real-World Scenario. We further evaluate the performance of our ClearAIR in real-world scenarios under various weather conditions, comparing it with several recent state-of-the-art methods. The RainDS (Quan et al. 2021) and Snow100K-real (Liu et al. 2018) datasets are used as test benchmarks. All methods are trained on the All-Weather task and directly evaluated on these real-world datasets. For Snow100K-real, where ground truth images are not available, we employ non-reference image quality assessment metrics, including MUSIQ (Ke et al. 2021) and NIQE (Mittal, Soundararajan, and Bovik 2012), for quantitative evaluation. As shown in Tab. 8, our method achieves the best performance on both RainDS and Snow100K-real datasets. In Fig. 7, it is clearly observed that WeatherDiff and WGWSNet fail to effectively suppress weather-related artifacts, while ClearAIR produces significantly clearer and more visually pleasing results. These quantitative and qualitative results demonstrate the superior practical effectiveness of ClearAIR in real-world All-Weather task.

Single Degradation Task. In this section, we evaluate the performance of ClearAIR under the One-by-One setting. As shown in Tab. 9, compared to the state-of-the-art (SOTA) task-specific denoising method ADFNet (Shen, Zhao, and Zhang 2023) and the SOTA general image restoration method FSNet (Cui et al. 2023), ClearAIR achieves superior results, outperforming them by 0.18/0.30 dB and 0.34/0.96 dB in PSNR, respectively, at a noise level of 15 on the CBSD68 and Urban100 datasets.

As presented in Tab. 10, ClearAIR also demonstrates the best performance in dehazing and deraining tasks. Specifically, it surpasses PromptIR by 0.60 dB and 1.48 dB in PSNR on the dehazing and deraining tasks, respectively. Even when compared to stronger single-task methods, ClearAIR still achieves improvements of 0.13 dB and 0.38 dB over DehazeFormer and DRSFormer, respectively. As illustrated in Fig. 8, images restored by our method retain relatively more texture details, leading to visually more pleasing outcomes. These results comprehensively validate the effectiveness and strong generalization ability of the proposed ClearAIR across different datasets and degradation types.

C. Limitation and Future Work

While ClearAIR advances All-in-One Image Restoration (AiOIR) by emulating the hierarchical coarse-to-fine process of Human Visual Perception (HVP), its current design has specific limitations for real-world application. The primary weakness is the inflexibility of its fixed perception pipeline, it lacks adaptability to complex, real-world scenarios where degradation types and intensities are spatially non-uniform. This is evidenced by its performance sensitivity to the processing order in ablation studies. Furthermore,

Method	RainDS			Snow100K-real	
	PSNR↑	SSIM↑	MUSIQ↑	MUSIQ↑	NIQE↓
AirNet (Li et al. 2022)	19.67	0.594	48.42	59.26	3.149
TransWeather (Valanarasu, Yasarla, and Patel 2022)	21.25	0.634	48.95	58.79	3.036
WeatherDiff (Özdenizci and Legenstein 2023)	22.62	0.659	55.04	60.47	2.951
PromptIR (Potlapalli et al. 2023)	22.83	0.654	53.17	60.96	2.949
WGWSNet (Zhu et al. 2023)	<u>22.97</u>	0.651	47.18	61.03	2.914
OneRestore (Guo et al. 2024)	22.74	<u>0.667</u>	53.91	<u>61.24</u>	<u>2.887</u>
ClearAIR	23.24	0.675	<u>54.38</u>	61.57	2.852

Table 8: Quantitative Results in Real-world All-Weather task.

Method	BSD68			Urban100			Kodak24		
	15	25	50	15	25	50	15	25	50
DnCNN (Zhang et al. 2017)	33.90	31.24	27.95	32.98	30.81	27.59	34.60	32.14	28.95
FFDNet (Zhang, Zuo, and Zhang 2018)	33.87	31.21	27.96	33.83	31.40	28.05	34.63	32.13	28.98
ADFNet (Shen, Zhao, and Zhang 2023)	34.21	31.60	28.19	34.50	32.13	28.71	34.77	32.22	29.06
DGUNet (Mou, Wang, and Zhang 2022)	33.85	31.10	27.92	33.67	31.27	27.94	34.56	32.10	28.91
Restormer (Zamir et al. 2022)	34.03	31.49	28.11	33.72	31.26	28.03	34.78	32.37	29.08
NAFNet (Chen et al. 2022a)	33.67	31.02	27.73	33.14	30.64	27.20	34.27	31.80	28.62
FSNet (Cui et al. 2023)	34.09	31.55	28.12	33.88	31.31	28.07	34.75	32.38	29.10
TAPE (Liu et al. 2022)	32.86	30.18	26.63	32.19	29.65	25.87	33.24	30.70	27.19
AirNet (Li et al. 2022)	34.14	31.48	28.23	34.40	32.10	28.88	<u>34.81</u>	<u>32.44</u>	29.10
IDR (Zhang et al. 2023a)	34.11	31.60	28.14	33.82	31.29	28.07	34.78	32.42	<u>29.13</u>
PromptIR (Potlapalli et al. 2023)	<u>34.34</u>	<u>31.71</u>	<u>28.49</u>	<u>34.77</u>	<u>32.49</u>	<u>29.39</u>	-	-	-
ClearAIR	34.39	31.73	28.52	34.84	32.54	29.41	34.90	32.52	29.27

Table 9: Comparison of denoising performance in the Single-task setting.

Method	Dehazing SOTS	Method		Deraining Rain100L
DehazeNet (Cai et al. 2016)	22.46/0.851	UMR (Yasarla and Patel 2019)		32.39/0.921
AODNet (Li et al. 2017)	20.29/0.877	MSPFN (Jiang et al. 2020)		33.50/0.948
DehazeFormer (Song et al. 2023)	<u>31.78/0.977</u>	DRSformer (Chen et al. 2023)		<u>38.14/0.983</u>
Restormer (Zamir et al. 2022)	30.87/0.969	Restormer (Zamir et al. 2022)		36.74/0.978
NAFNet (Chen et al. 2022a)	30.98/0.970	NAFNet (Chen et al. 2022a)		36.63/0.977
FSNet (Cui et al. 2023)	31.11/0.971	FSNet (Cui et al. 2023)		37.27/0.980
AirNet (Li et al. 2022)	23.18/0.900	AirNet (Li et al. 2022)		34.90/0.977
PromptIR (Potlapalli et al. 2023)	31.31/0.973	PromptIR (Potlapalli et al. 2023)		37.04/0.979
ClearAIR	31.91/0.978	ClearAIR		38.52/0.985

Table 10: Comparison of dehazing and deraining performance in the Single-task setting.

key components exhibit blind spots: the semantic guidance module struggles with inaccurate region masking under extreme low-visibility conditions, and the internal detail enhancement relies on a perceptually uninformed data augmentation strategy, which can lead to suboptimal recovery of fine details.

To address these issues, a promising path forward is the deep integration of a Just Noticeable Difference (JND) (Chou and Li 1995) mechanism. This integration would shift the paradigm from merely mimicking the HVP workflow to

embedding its fundamental perceptual laws. The envisioned JND-aware framework would employ a dynamic controller to adaptively route the restoration process based on perceptual thresholds and apply JND-weighted mechanisms to focus computational resources on perceptually critical regions. This evolution towards a perceptually-adaptive system is key to achieving significant gains in robustness and visual fidelity for complex, real-world degradations.

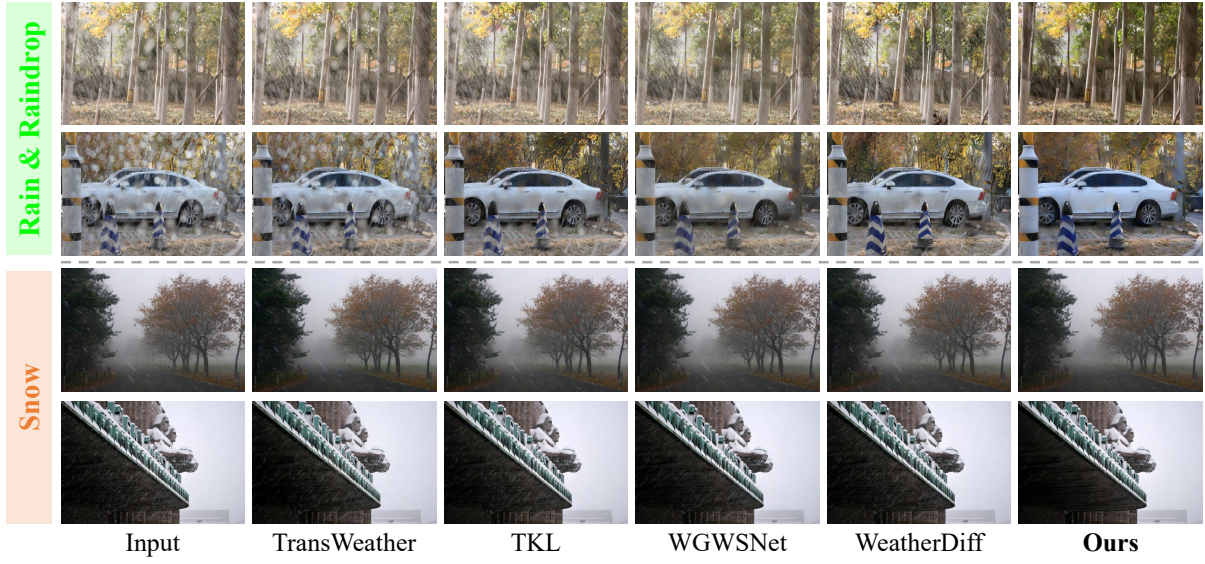


Figure 7: Visual comparisons of ClearAIR against state-of-the-art All-in-One methods under real-world All-Weather task on RainDS and Snow100K-real datasets (from top to bottom). Zoom-in for best view.

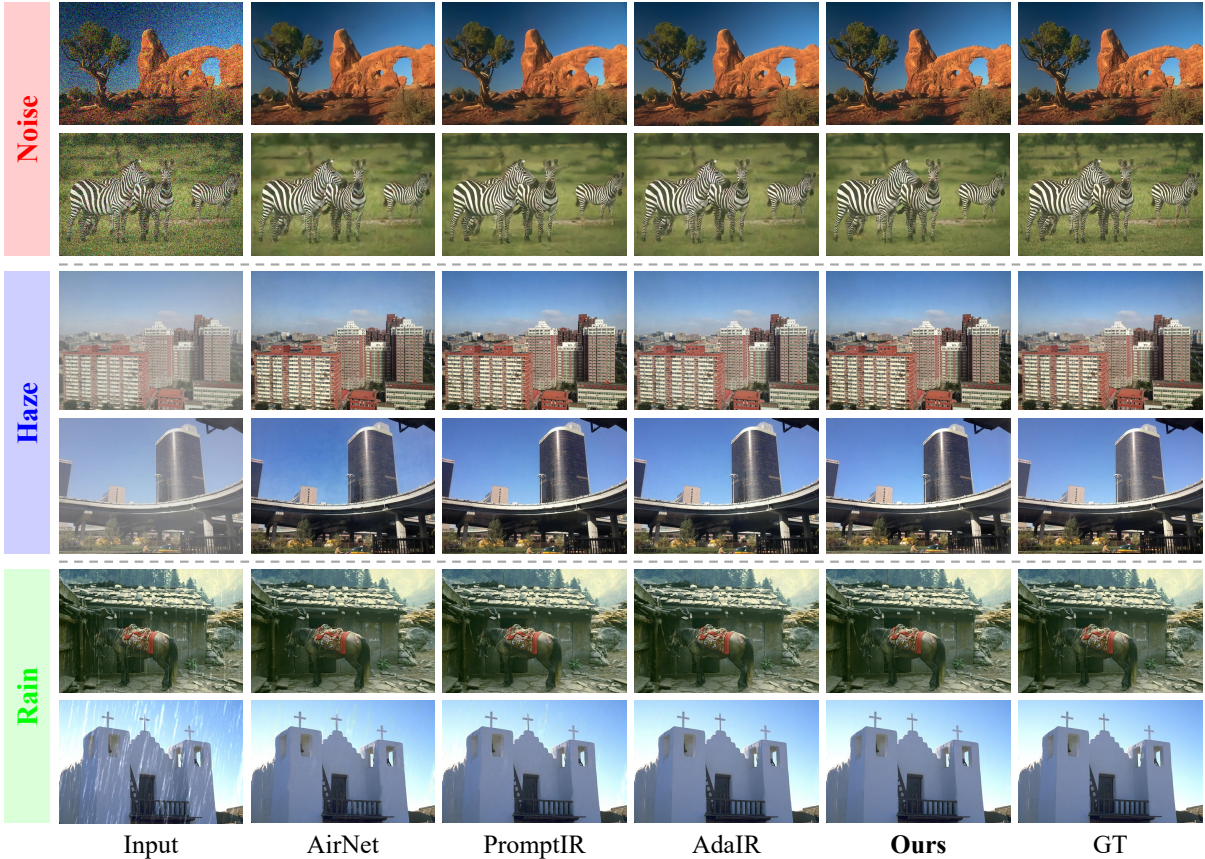


Figure 8: Visual comparisons of ClearAIR against state-of-the-art All-in-One methods under Single Degradation task on BSD68, SOTS-Outdoor, and Rain100L datasets (from top to bottom). Zoom-in for best view.

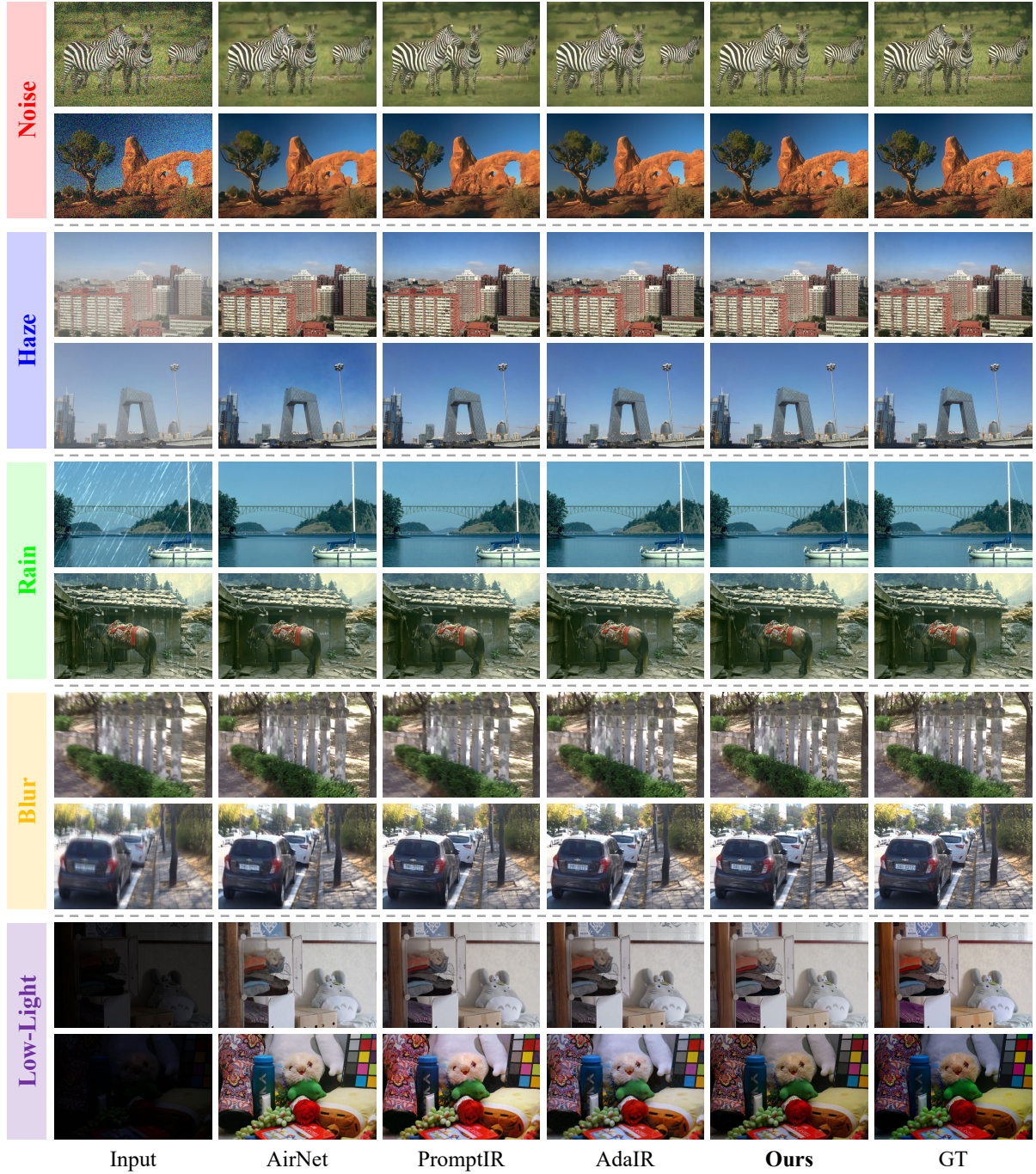


Figure 9: Visual comparisons of ClearAIR against state-of-the-art All-in-One methods under Five Degradation task on BSD68, SOTS-Outdoor, Rain100L, GoPro and LOL datasets (from top to bottom). Zoom-in for best view.